ACS APPLIED MATERIALS & INTERFACES

www.acsami.org

Research Article

Effective Ru/CNT Cathode for Rechargeable Solid-State Li−CO_2 Batteries

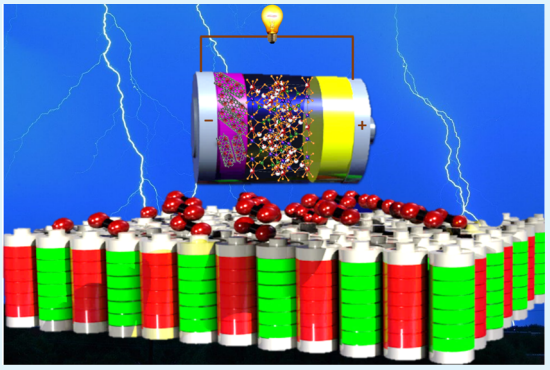
Kirankumar Venkatesan Savunthari, Chien-Hung Chen, You-Ruei Chen, Zizheng Tong, Kevin Iputera, Fu-Ming Wang, Chun-Chuan Hsu, Da-Hua Wei,* Shu-Fen Hu,* and Ru-Shi Liu*

Cite This: *ACS Appl. Mater. Interfaces* 2021, 13, 44266−44273

Read Online

ACCESS | Metrics & More | Article Recommendations | Supporting Information

ABSTRACT: An effective Ru/CNT electrocatalyst plays a crucial role in solid-state lithium−carbon dioxide batteries. In the present article, ruthenium metal decorated on a multi-walled carbon nanotubes (CNTs) is introduced as a cathode for the lithium−carbon dioxide batteries with $Li_{1.5}Al_{0.5}Ge_{1.5}(PO_4)_3$ solid-state electrolyte. The Ru/CNT cathode exhibits a large surface area, maximum discharge capacity, excellent reversibility, and long cycle life with low overpotential. The electrocatalyst achieves improved electrocatalytic performance for the carbon dioxide reduction reaction and carbon dioxide evolution reaction, which are related to the available active sites. Using the Ru/CNT cathode, the solid-state lithium−carbon dioxide battery exhibits a maximum discharge capacity of 4541 mA h g^{-1} and 45 cycles of battery life with a small voltage gap of 1.24 V compared to the CNT cathode (maximum discharge capacity of 1828 mA h g^{-1}, 25 cycles, and 1.64 V as voltage gap) at a current supply of 100 mA g^{-1} with a cutoff capacity of 500 mA h g^{-1}. Solid-state lithium−carbon dioxide batteries have shown promising potential applications for future energy storage.



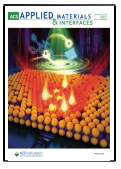
KEYWORDS: *Ru/CNT cathode, Ru nanoparticles, LAGP solid electrolyte, solid-state Li−CO_2 batteries, and Li-metal anode*

INTRODUCTION

Solid-state lithium batteries (SSLBs) are favorable for future energy storage applications. The importance of SSLBs emerges from the likelihood to utilize high-voltage cathodes and high-capacity anodes (Li metal) without compromising safety.[1,2] At present, rechargeable lithium−carbon dioxide batteries (LCBs) are gaining importance worldwide because of their capability to capture carbon dioxide and change it into energy.[3−7] Furthermore, LCBs have a 1876 W h kg^{-1} theoretical energy density,[5] which remains consistent with the electrochemical process of lithium carbonate formation and deformation ($4Li + 3CO_2 \leftrightarrow 2Li_2CO_3 + C$) amid the discharge−charge reactions.[5−12] These LCBs utilize organic liquid electrolytes to transfer lithium ions during the electrochemical process.[11] Nonetheless, these batteries possess some disadvantages, including liquid leakage and flammability, because of the presence of liquid organic electrolytes. Therefore, creating solid-state Li−CO_2 batteries (SSLCBs) is suggested to address these detriments.[9,13] However, SSLCBs have high mechanical strength and high thermal stability, which can avoid ignitability and liquid leakage.

Solid-state electrolytes (SSEs) have several criteria, such as low electronic conductivity, high ionic conductivity, and suitable electrochemical and chemical stability against coupling electrodes.[14] For commercial uses, cost-effective and ecologically benign compounds are suitable for the practical development of SSLCBs. In particular, inorganic solid-state electrolytes (ISSEs) play a crucial role in SSLBs. ISSE has various structures, such as NASICON, garnet, thio-LISICON, LISICON, anti-perovskite, perovskite, sulfide-type glass/ceramic, LiPON, and hydrides, which have been intensively studied.[2,15−21] Among all ISSEs, sulfide-type electrolytes are reactive to moisture, and they must be fabricated under inactive air, which implies that they are not applicable for Li−O_2 and LCBs.[9,20,22] On the contrary, garnet solid electrolytes are also unstable against moisture,[20,22] which increases their fabrication cost. Conversely, the NASICON-type ISSEs also show high lithium-ion conductivity, which could be obtained for $Li_{1+x}Al_xGe_{2-x}(PO_4)_3$ (LAGP) and $Li_{1+x}Al_xTi_{2-x}(PO_4)_3$ (LATP). In addition, ceramic-type LATP and LAGP have shown great potential, where the Li-transport boundary at grain limits could be alleviated.[14] LAGP solid electrolytes possess high stability in CO_2, which is appropriate for SSLCBs.

Received: June 12, 2021
Published: September 8, 2021



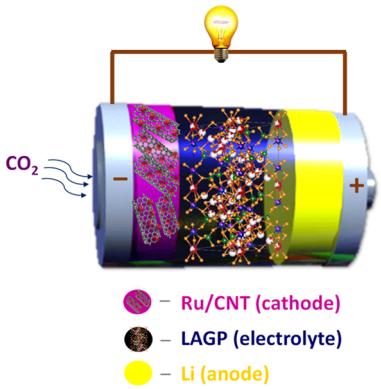
Downloaded via NATL TAIWAN UNIV on November 2, 2021 at 06:13:10 (UTC).
See https://pubs.acs.org/sharingguidelines for options on how to legitimately share published articles.

© 2021 American Chemical Society

For LCBs, carbonaceous catalysts are widely applied as cathodes due to their large surface area and high electronic conductivity.[5,9,22−24] However, using pure carbonaceous catalysts always results in high overpotential. Therefore, selecting suitable cathode materials to enhance the rechargeability of LCBs is important. To date, nanocatalysts have been intensively studied for rechargeable LCBs such as RuO_2@single-walled CNTs(SWCNTs),[9] Ru/NiO@Ni/CNTs,[25] covalent organic framework-Ru@CNTs,[26] CNT@RuO_2,[27] and TiO_2-nanoparticles@CNTs/carbon nanofibers.[28] Among the nanocatalysts, the ruthenium (Ru)-based cathode shows good electrocatalytic activity for the decomposition of Li_2CO_3.[5,9,26,29,30] Liu's[31,32] and Zhou's[9] groups achieved a maximum decomposition of Li_2CO_3 by loading Ru metal on a CNT and RuO_2 on a SWCNT, thereby diminishing the charge potential of the LCBs. Du et al.[9] reported that the RuO_2/SWCNT/LAGP cathode showed a stable cycling behavior over 30 cycles at 60 °C with LAGP@Ge electrolyte for all-SSLCBs. In addition, Wang et al.[13] proved that the all-SSLCBs can run for 70 cycles when using the CNT cathode and polymer SSE with a garnet filler. However, the Ru/CNT cathode with LAGP electrolyte has not yet been introduced in SSLCBs.

Herein, we introduced Ru nanoparticles (NPs) on CNTs as a cathode and LAGP SSE for SSLCBs at room temperature (as shown in Scheme 1). The cathode materials show a tiny crystalline size and a high BET surface area, which results in maximum discharge capacity (4541 mA h g^{-1}), a small voltage gap (1.24 V), and 45 cycles of battery life with 500 mA h g^{-1} limiting capacity at 100 mA g^{-1} current density. Scheme 1 represents SSLCBs having a porous cathode Ru/CNT, anode Li metal, and LAGP SSE. The effective Ru metal catalyst and CNTs significantly improve the flexible formation and deformation of the discharge compound. Consequently, the SSLCBs having the Ru/CNT cathode reach the superb maximum discharge capacity, a small potential gap, and an extraordinary cycling performance.

Scheme 1. Schematic Illustration of the SSLCBs



EXPERIMENTAL METHODS

Fabrication of Cathodes. The Ru/CNT cathode was fabricated via the reflux technique described in previous studies.[32] In the fabrication of cathodes (CNTs and Ru/CNTs), 36 mg of CNT or Ru/CNT powder and 4 mg of PVDF (polyvinylidene fluoride) binder were added in a weight ratio of 9:1 with 1000 μL of NMP (*N*-methyl-2-pyrrolidinone) solvent via a ball-milling machine (Retsch PM 100) for 30 min. Then, 10 μL of the as-prepared cathode was drop-casted evenly on the carbon paper, which was further dried at 80 °C in a vacuum oven for 12 h. The weight loading of cathode-active materials (CNT or Ru/CNT) was around 0.15 to 0.20 mg.

Inorganic Solid-State Electrolyte. LAGP pellets were bought from Shenzhen Kejing Star Technology Company Ltd., Shenzhen, China (diameter = 12 mm and thickness = 0.3 mm). Before coin cell assembly, the LAGP was carefully polished on both sides (Taiwan Nakazawa polishing machine).

Coin Cell Fabrication and Electrochemical Analysis. The SSLCBs were fabricated using coin cells (CR2032-type) with holes on the cathode side (Ar-filled glovebox and <1 ppm of O_2 and H_2O). The battery coin cell was composed of a CNT or Ru/CNT cathode, one drop of 1 M lithium bis(trifluoromethanesulfonyl)imide in tetraethylene glycol dimethyl ether (Sigma-Aldrich: LiTFSI + TEGDME), polished LAGP SSE, and anode Li metal (diameter = 10 mm). After assembling, the battery coin cells were moved to a homemade glass bottle. Afterward, CO_2 (2N, 99%) was purged in the bottle for electrochemical tests.

SSLCBs were analyzed using an AcuTech battery tester. Discharge and charge tests of both cathodes (CNT and Ru/CNT) were conducted with the fixing capacity (500 mA h g^{-1}) at a current density (100 mA g^{-1}) using a voltage range of 2.2 to 4.5 V (vs Li^+/Li). Electrochemical impedance spectra (EIS) of Au/LAGP/Au samples (0.1 to 10^6 Hz) were recorded.

Characterization. The pure phase of cathode materials and SSE (Rietveld refinements were confirmed by TOPAS 4.2) was obtained by powder X-ray diffraction (XRD, Cu Kα radiations λ = 1.54178 Å, Bruker D2 PHASER). Raman spectra were recorded using Thermo Fisher Scientific DXR. Morphologies of cathode materials were determined by field-emission scanning electron microscopy (FE-SEM, ZEISS SIGMA) and transmission electron microscopy (TEM, JEOL JEM-2100F). The BET (Brunauer−Emmett−Teller) surface area and X-ray absorption spectra (XPS) were recorded using Micromeritics ASAP2020 ASAP2010 and Thermo Scientific, Theta probe, 113R, 2008 5, respectively. Images of the as-prepared sample, first discharge and first recharge of Ru/CNT cathode materials, and those after 45 cycles were recorded using the 24A1 XPS and 01C1 extended X-ray absorption fine structure fitting beamline of (EXAFS was resolved on Artemis) the National Synchrotron Radiation Research Center, Hsinchu, Taiwan.

RESULTS AND DISCUSSION

Cathodes of CNTs and Ru/CNTs. The crystal conformation of CNT and Ru/CNT cathodes was confirmed by powder XRD. As displayed in Figure 1a, the diffraction patterns at 2θ = 25.35, 42.55, 52.84, and 78.0° are corresponding to the (002), (100), (004), and (110) planes, respectively, which indicated the presence of the CNT. No impurities in the peaks are noted in the XRD pattern, which shows the existence of a pure single-phase CNT. Metallic Ru is observed in the Ru/CNT (Figure 1a), as shown in its XRD pattern, where the 2θ peaks at 38.42, 42.19, 44.04, 58.38, 69.47, and 78.47° correspond to the (110), (002), (101), (102), (110), and (103) planes of hexagonal metallic Ru (PDF#06-0663). In addition, the Ru/CNT sample confirmed the presence of a CNT and Ru (marked with # for CNT and * for Ru metal). The average crystalline size (D) of the Ru/CNT cathode can be estimated from full-width at half maximum of various planes using Debye−Scherrer's formula.[25] The average crystalline size of the fabricated cathode was approximately 3.16 nm for the Ru/CNT samples. Raman spectra of the Ru/CNT cathode (Figure S1) showed two typical peaks located at 1344 and 1554 cm^{-1}, corresponding to the disordered carbon and graphitic carbon, respectively.[5,33] Furthermore, the BET surface area of the pure CNT was 260 m^2 g^{-1}, and for the Ru/CNT sample, it was 268 m^2 g^{-1}. The BET surface area of the CNT and Ru/CNT are comparable, indicating that the large surface area of the Ru/CNT is mainly contributed by CNT.

https://doi.org/10.1021/acsami.1c11000
ACS Appl. Mater. Interfaces 2021, 13, 44266−44273

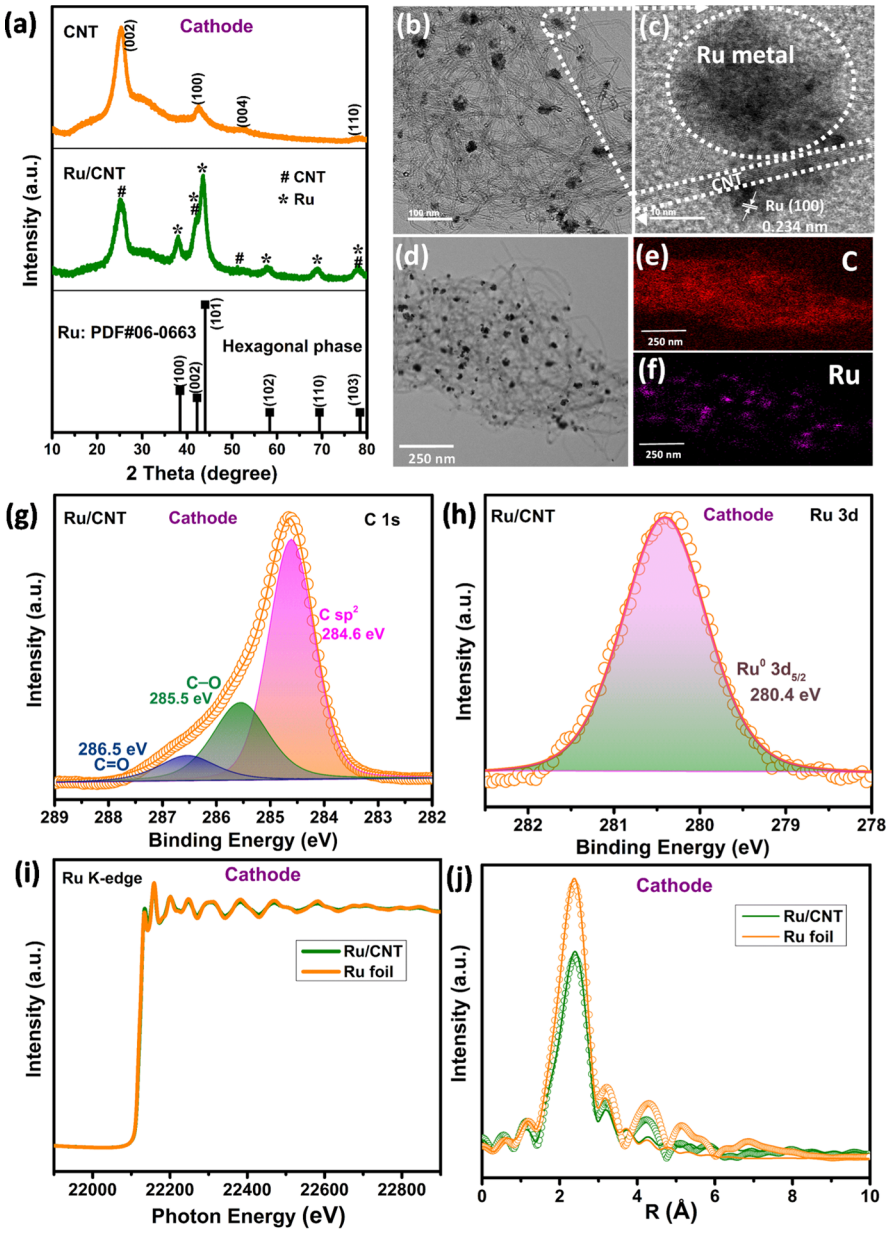


Figure 1. (a) Powder XRD results of the CNT and Ru/CNT cathode. (b–d) TEM images and (d–f) EDX element mapping of (e) carbon and (f) ruthenium using the Ru/CNT cathode. Synchrotron XPS results of (g) carbon 1s and (h) ruthenium 3d using the Ru/CNT cathode. (i) Synchrotron XANES spectrum of the Ru foil and Ru/CNT cathode. (j) *R*-space of Fourier transformed k^3-weighted synchrotron EXAFS signals and best fit of the Ru foil and Ru/CNT cathode.

The enlarged BET surface area is favorable for improving the catalytic efficiency.

The Ru/CNT catalyst SEM images display that ruthenium metal is homogeneously distributed on the CNT (Figure S2a). The SEM shows the secondary particles with a size of 17–18 nm. The secondary particles are self-assembled using Ru nanocrystals with a particle size of 3.16 nm, which is calculated using Scherrer's equation. The presence of Ru and carbon (C) was proved by energy dispersive X-ray analysis (EDAX) analysis, and SEM elemental mapping images are shown in Figures S2b–f. The TEM images of the Ru/CNT cathode illustrate that Ru metal (dark spots) is consistently distributed on the CNT (Figure 1b). As shown in Figure 1c, the Ru metallic lattice distance was 0.234 nm based on the (100) plane of hexagonal metallic Ru (PDF#06-0663). The presence of Ru and C was confirmed by EDAX (Figure S3a) and elemental mapping (Figure 1d–f) images. Furthermore, the ruthenium NPs have an average particle size of around 3.5 nm and are uniformly supported on the CNT surface (Figure S3b). The Ru/CNT cathode possesses a superb electron conductivity, and Ru metal has excellent electrocatalytic performance during the appearance and disappearance of lithium carbonate in LCBs.

The surface chemistry and oxidation state of a cathode (Ru/CNT) were estimated by synchrotron XPS. The carbon 1*s* peak located at 284.6, 285.5, and 286.5 eV might be attributed to C sp^2, C–O, and C=O, respectively (Figure 1g).[31,32] The XPS spectra of Ru 3*d* (Figure 1h) peak at 280.4 eV, corresponding to Ru^0 $3d_{5/2}$.[5] The C sp^2 and Ru^0 play a significant part in enhancing the electronic conductivity of the cathode. The oxidation state and coordination environment of the Ru/CNT catalyst were examined by EXAFS analysis.

https://doi.org/10.1021/acsami.1c11000
ACS Appl. Mater. Interfaces 2021, 13, 44266–44273

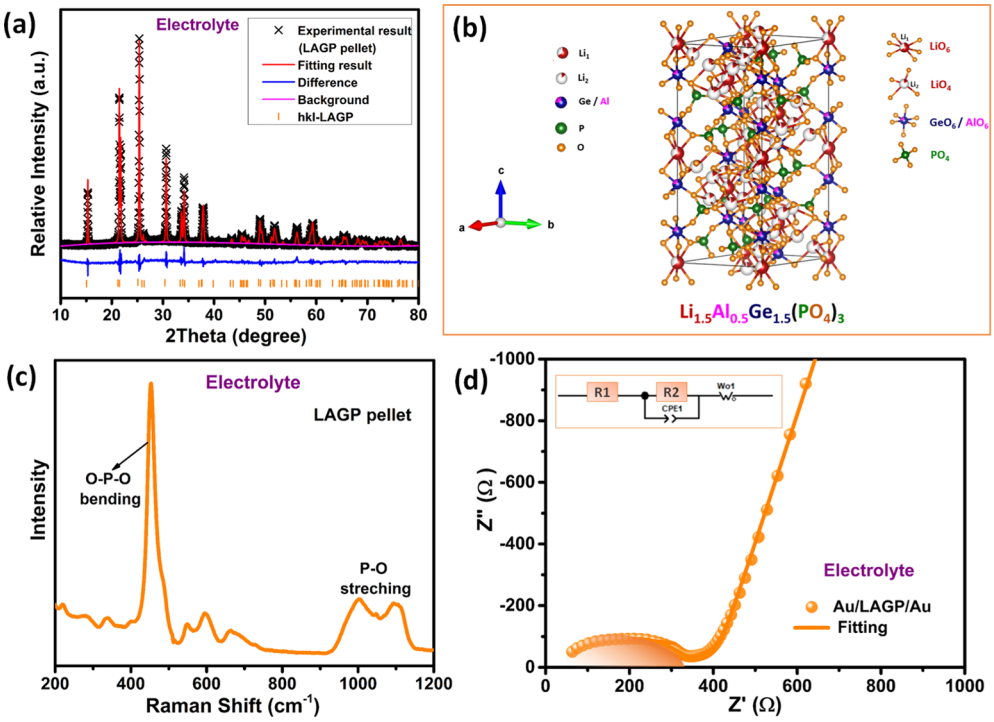


Figure 2. (a) Rietveld refinement XRD pattern, (b) crystal structure, and (c) Raman spectra of LAGP SSE. (d) Nyquist plot of the LAGP pellet measured with Au/LAGP/Au at room temperature.

Figure 1i shows that the Ru K-edge X-ray absorption near-edge spectroscopy (XANES) data of the cathode (Ru/CNT) were related to those of the Ru foil. No major difference was observed between the Ru foil and Ru/CNT cathode in Ru K-edge XANES analysis.[34] The Ru K-edge XANES peak proved that the oxidation state of Ru^0 corresponded to the location of the absorption edge. Fourier transform (FT) *R*-space EXAFS data of the Ru foil and Ru/CNT cathode (Figure 1j) and fitting values are tabulated in Table S1, thereby showing the presence of Ru−Ru coordination in the Ru foil [bond length ∼ 2.67 Å and coordination number (C.N.) ∼ 8.176] and Ru/CNT cathode (bond distance ∼ 2.67 Å and C.N. ∼ 7.464). The reduced C.N. is an advantage for the ruthenium atom surface to absorb carbon dioxide, thereby leading to a carbon dioxide reduction reaction (CO_2RR) during the discharge cycle.[35] Furthermore, the Ru atom surface with a smaller C.N. might serve as the active site of the carbon dioxide evolution reaction (CO_2ER).[32,35]

LAGP SSE. The Rietveld refinement results display the rhombohedral crystal structure: space group $\bar{R}3d$ with the NASICON-type LAGP crystal system. The calculated refinement XRD pattern is shown in Figure 2a. The different structural parameters and profile parameters are tabulated in Tables S2 and S3. LAGP is primarily composed of $LiGe_2(PO_4)_3$ (LGP) with a NASICON-type system, among which Ge^{4+} ions are partially substituted with Al^{3+} ions. LAGP is composed of AlO_6/GeO_6 octahedra and PO_4 tetrahedra, which are associated with each other to create a 3D network structure.[36,37] As shown in Figure 2b, the Li sites in the LAGP structure are of two types [Li(1) and Li(2)]. In LAGP, AlO_6/GeO_6 octahedra and PO_4 tetrahedra create a rhombohedral crystal structure. Ge^{4+} is partly replaced with a smaller Al^{3+} ion to decrease the unit cell dimensions, thereby promoting the densifying impact and improving ionic conductivity.[37] Raman spectra were performed to examine the bonding and local structure of the LAGP SSE. Figure 2c displays that the number of bands in the LAGP pellet is in the range of 300−530, 550−650, and 900−1200 cm^{-1}, which could be assigned to the bending, symmetric, and anti-symmetric stretching, respectively.[37] As shown in Figure 2d, the EIS of Au/LAGP/Au achieved a total resistance of 322.96 Ω and an ionic conductivity of 0.7 mS cm^{-1} at room temperature. The good ionic conductance and small resistance of LAGP are favorable in the application of SSLCBs.

Electrochemical Analysis. The electrochemical activity of CNT and Ru/CNT cathodes for the SSLCBs with the LAGP SSE and Li-metal anode was analyzed. CV (cyclic voltammetry) measurements to explore the catalytic performance of CNT and Ru/CNT catalysts in SSLCBs from 4.5−2 V are given in Figure 3a. The peak currents for the anode and cathode were greater for the Ru/CNT cathode as compared to the pure CNT cathode, demonstrating that the CO_2RR and CO_2ER reactions were better to study the Ru/CNT catalyst than the pure CNT catalyst for the SSLCBs. Figure 3b shows the full discharge−recharge measurements of pure CNT and Ru/CNT cathodes for the SSLCBs at 100 mA g^{-1} current density. From Figure 3b, the Ru/CNT cathode conveyed a maximum discharge capacity of 4541 mA h g^{-1} at a voltage stage of 2.50 V, which is comparatively greater than that of the pure CNT cathode (1828 mA h g^{-1} with a voltage platform 2.32 V). It could be noticed that the SSLCBs using the pure CNT and Ru/CNT catalysts exhibit a maximum charge capacity of 1832 and 4425 mA h g^{-1} with the charging platform at 4.25 and 4.02 V, respectively. The higher discharge/charge capacity and lower discharge/charge platform of the Ru/CNT catalyst showed the superb electrocatalytic activity of Ru NPs in SSLCBs. Figure 3c,d displays the discharge−charge cycling performance of cathodes (CNT and Ru/CNT) with a 500 mA h g^{-1} limiting capacity and 100 mA g^{-1} current density at room temperature (limiting voltage

https://doi.org/10.1021/acsami.1c11000
ACS Appl. Mater. Interfaces 2021, 13, 44266−44273

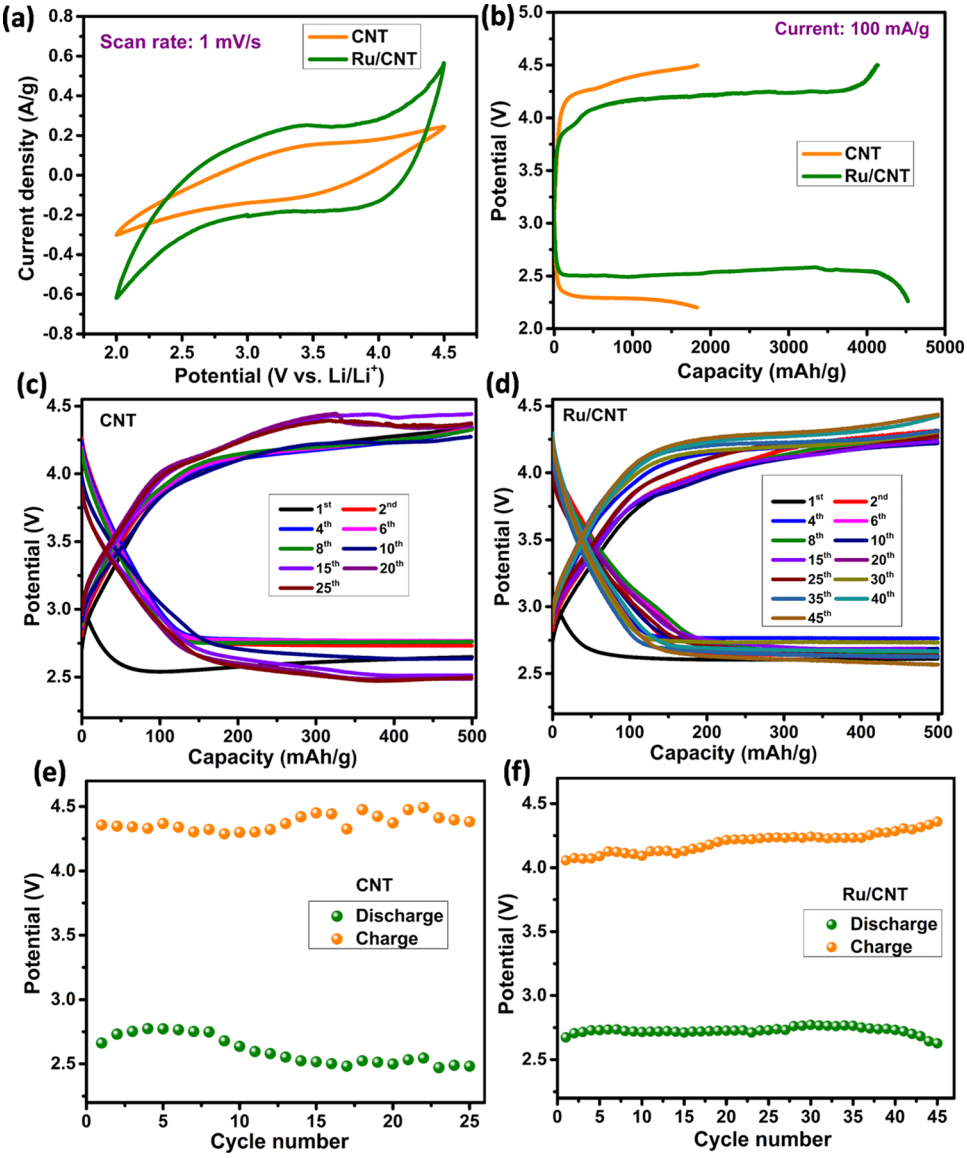


Figure 3. (a) CV measurements and (b) maximum discharge capacity of the SSLCBs using CNT and Ru/CNT samples. Cycling (discharge−charge cycle) performance of (c) CNT and (d) Ru/CNT catalysts and overpotential performance (discharge−charge potential vs cycle number) of (e) CNT and (f) Ru/CNT samples for SSLCBs with 500 mA h g^{-1} fixed capacity and 100 mA g^{-1} current density at room temperature.

range of 2.2−4.5 V). The CNT catalyst battery can only stand for 25 cycles with large overpotential (Figure 3c). The Ru/CNT catalyst battery can run efficiently for 45 cycles with low overpotential, which is better than the CNT catalyst battery (Figure 3d). These results indicated that the catalyst with a large surface area can run for long cycles with low overpotential. The excellent cycling behavior of the Ru/CNT cathode battery might result from a high BET surface area and superior electronic properties.

The CNT cathode shows the maximum discharge platform at 2.68 V and the charging platform at 4.32 V, representing a potential gap of 1.64 V (first cycle, Figure 3e). As shown in Figure 3f, the Ru/CNT cathode has a discharge stage at 2.80 V and a recharge stage at 4.02 V, indicating its small potential gap of 1.24 V (first cycle) compared with the CNT cathode. This result indicates the favorable catalytic ability of the Ru/CNT for CO_2RR and CO_2ER reactions. The Ru/CNT cathode battery shows not only good cycling stability but also keeps constant overpotential discharge and charge levels until 38 cycles. These results confirmed that the strong synergistic impact of the ruthenium nanoparticles and CNT resulted in the great catalytic performance of the Ru/CNT cathode, thereby reducing the overpotential and promoting the cycling stability of SSLCBs. The overpotential of charging voltages slightly increases after 9 (CNT) and 39 (Ru/CNT) cycles from 4.31 to 4.48 and 4.21 to 4.37 V, respectively, because of the formation and deformation of insoluble lithium carbonate, respectively (Figure 3e,f).[5] In comparison with previous results, the present Ru/CNT cathode shows high cycling stability and low overpotential for SSLCBs (Table S4).

Stability Studies of the Cathode and Electrolyte. In studying the stability of the catalytic performance of cathodes (CNT and Ru/CNT), the continuous discharge−charge cycle of SSLCBs was shown with a limiting capacity of 500 mA h g^{-1} and a current density of 100 mA g^{-1}. Ex situ analysis of powder XRD, Raman, XPS, and XANES was presented to display the reversible formation and deformation of Li_2CO_3 amid the discharge and charge cycle. The digital images of solid-state

https://doi.org/10.1021/acsami.1c11000
ACS Appl. Mater. Interfaces 2021, 13, 44266−44273

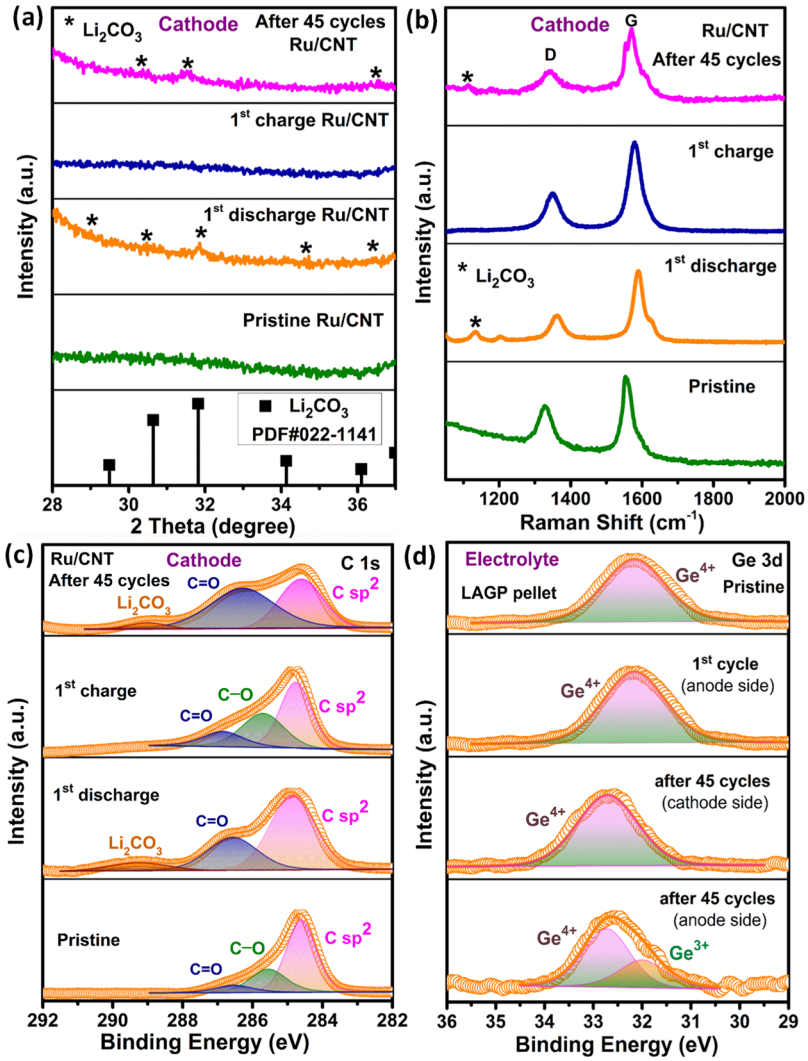


Figure 4. Ru/CNT catalyst: pristine, first discharge, first recharge, and after 45 cycles (charge) in SSLCBs measured with (a) powder XRD, (b) Raman, and (c) XPS results of C 1s. (d) XPS spectra of germanium (Ge 3d): pristine, first cycle on the anode side, and after 45 cycles on the cathode and anode sides using LAGP SSLCBs.

batteries were disassembled at the first cycle and after 45 cycles when the Ru/CNT cathode was used for LAGP SSLCBs (Figure S4). After the first discharge, the XRD pattern could be attributed to lithium carbonate (PDF#22-1141), confirming the deposition of lithium carbonate on the Ru/CNT samples (Figure 4a). After the first recharge, all the peaks of lithium carbonate vanished, confirming the deformation of lithium carbonate on the cathode side (Figure 4a). These results indicate that the CO_2RR occurs during the discharge cycle and CO_2 is diminished by Li metal to produce Li_2CO_3. During the charging cycle, the discharge products of Li_2CO_3 were decomposed to form CO_2, particularly the CO_2ER. The Ru metal NPs could enhance the electrocatalytic activity of SSLCBs.[35] After charging 45 cycles of Ru/CNT (Figure 4a) cathodes and 25 cycles of CNT (Figure S5) cathodes on the surface, the Li_2CO_3 discharge compounds of SSLCBs were observed. These results indicated that lithium carbonate, which was created amid the discharge cycle, was not completely deformed amid recharging cycles. The poor cycling performance (Figure 3c,d) resulted in a dramatic loss of interaction between lithium carbonate and the cathodes (CNT and Ru/CNT) at the end of the charging steps.[9]

Raman spectroscopy (Figure 4b) was performed to observe the discharge product of Li_2CO_3. For the first discharge of the Ru/CNT cathode, a weak peak presented at 1096 cm^{-1} was ascribed to lithium carbonate.[5,31] Li_2CO_3 decomposition and deposition of the Ru/CNT catalyst occurred during the first recharge and after 45 charge cycles. In addition, the XPS spectra of the Ru/CNT catalyst C 1s at the as-prepared powder, first discharge, first charge, and after charging 45 cycles are displayed in Figure 4c. Compared with the C 1*s* spectrum of the pristine cathode, a new peak attributing to lithium carbonate at 289.5 eV occurs in the first discharge cathode and deformation occurs after the subsequent first charge.[5,27] These results demonstrate the reversible appearance and disappearance of the Li_2CO_3 peak during the discharge–charge cycles, which is in agreement with Raman and XRD studies. Furthermore, the Ru/CNT catalyst shows lithium carbonate accumulation after 45 cycles of charging steps. The XANES data of ruthenium K-edge of the cathode were collected to analyze the atomic and electronic properties of the cathode amid the first discharge and recharge in the SSLCBs (Figure S6). Based on the results, no changes were observed in

https://doi.org/10.1021/acsami.1c11000
ACS Appl. Mater. Interfaces 2021, 13, 44266–44273

the oxidation state of the Ru catalyst, demonstrating the stability of the cathode during the cycles.[32,35]

The *in situ* GC−MS (gas chromatography−mass spectrometry) analysis confirmed the CO_2 evolution during the recharging process (Figure S7). The experimental procedures were followed using previous reports.[32] During the recharging steps, the relating gas evolution profiles of the carbon dioxide (m/z = 44; CO_2) and oxygen (m/z = 32; O_2) fragment for SSLCBs using the Ru/CNT catalyst show the evolution of carbon dioxide happening in the electrochemical battery system and negligible conspicuous modification in the O_2 fragment evolution curves (Figure S7). *In situ* GC−MS data prove the effective electrocatalytic activity of the Ru/CNT cathode for the flexible deformation of lithium carbonate to carbon dioxide amid the recharging reactions of SSLCBs. The presence of C discharge compounds was confirmed utilizing XRD, Raman, and XPS analysis; only carbon dioxide gas evolution was identified (oxygen gas was not identified) amid the recharging cycle (Figure S7).

As shown in Figures S4 and 4d, the LAGP pellet in the first cycle shows fresh and the same oxidation state Ge^{4+} like pristine. In this case, after 45 cycles, the LAGP electrolyte was cracked with the black dots found on the SSE surface, and it formed a mixed conducting interphase. XPS analysis proved that Ge^{4+} was reduced to Ge^{3+} on the anode side after 45 cycles and no changes were observed on the cathode side after charging 45 cycles (Figure 4d). These results suggest the substantial side reactions between the lithium metal anode and LAGP SSE (direct contact), which create the interphase from high resistance to ionic transport and leads to lithium penetration into LAGP, thereby cracking the SSE.[21] Subsequently, the fractured LAGP SSE and Li anode penetration reduce the battery performance.

CONCLUSIONS

We successfully developed the SSLCBs using a cathode Ru/CNT, NASICON-type LAGP SSE, and lithium metal anode. The large surface area and good electronic properties of the Ru/CNT cathode enhance the electrochemical process. The Ru/CNT cathode shows an excellent discharge capacity of 4541 mA h g^{-1}, 45 cycles of battery life, and a low overpotential of 1.24 V between the discharge and charge processes at 100 mA g^{-1} current density with 500 mA h g^{-1} cutoff capacity. Hence, the cathode of Ru/CNT is considered as a superb cathode for SSLCBs to date. The flexible formation and deformation of Li_2CO_3 discharge compounds are confirmed *via in situ* and *ex situ* instrumental analysis. This work provides insights into the improvement of cathode electrocatalysts for SSLCBs and future devices of energy storage.

ASSOCIATED CONTENT

Supporting Information

The Supporting Information is available free of charge at https://pubs.acs.org/doi/10.1021/acsami.1c11000.

Raman spectra, SEM-EDAX, elemental mapping, TEM-EDAX, optical images, powder XRD pattern, XANES spectrum of the Ru/CNT cathode (pristine, first discharge, and first charge), in situ GC−MS results, fitting results for Ru K-edge EXAFS spectra, Rietveld refinement values, and literature comparison results (PDF)

AUTHOR INFORMATION

Corresponding Authors

Da-Hua Wei − *Department of Mechanical Engineering and Graduate Institute of Manufacturing Technology, National Taipei University of Technology, Taipei 106, Taiwan;* orcid.org/0000-0001-7603-3739; Email: dhwei@ntut.edu.tw

Shu-Fen Hu − *Department of Physics, National Taiwan Normal University, Taipei 116, Taiwan;* orcid.org/0000-0001-9561-8206; Email: sfhu.hu@ntnu.edu.tw

Ru-Shi Liu − *Department of Chemistry, National Taiwan University, Taipei 106, Taiwan;* orcid.org/0000-0002-1291-9052; Email: rsliu@ntu.edu.tw

Authors

Kirankumar Venkatesan Savunthari − *Department of Chemistry, National Taiwan University, Taipei 106, Taiwan;* orcid.org/0000-0003-2367-0501

Chien-Hung Chen − *Department of Mechanical Engineering and Graduate Institute of Manufacturing Technology, National Taipei University of Technology, Taipei 106, Taiwan*

You-Ruei Chen − *Department of Physics, National Taiwan Normal University, Taipei 116, Taiwan*

Zizheng Tong − *Department of Chemistry, National Taiwan University, Taipei 106, Taiwan*

Kevin Iputera − *Department of Chemistry, National Taiwan University, Taipei 106, Taiwan*

Fu-Ming Wang − *Graduate Institute of Applied Science and Technology and Sustainable Energy Center, National Taiwan University of Science and Technology, Taipei 106, Taiwan; R&D Center for Membrane Technology and Department of Chemical Engineering, Chung Yuan Christian University, Taoyuan 320, Taiwan;* orcid.org/0000-0003-4407-3554

Chun-Chuan Hsu − *Graduate Institute of Applied Science and Technology, National Taiwan University of Science and Technology, Taipei 106, Taiwan*

Complete contact information is available at: https://pubs.acs.org/10.1021/acsami.1c11000

Notes

The authors declare no competing financial interest.

ACKNOWLEDGMENTS

This work was financially supported by the Ministry of Science and Technology, Taiwan (contract numbers: MOST 107-2113-M-002-008-MY3, MOST 109-2113-M-002-020-MY3, MOST 109-2112-M-003-011, MOST 110-2112-M-003-016, and MOST 110-3116-F-011-002).

REFERENCES

(1) Janek, J.; Zeier, W. G. A Solid Future for Battery Development. *Nat. Energy* **2016**, *1*, 1−4.

(2) Xiong, S.; Liu, Y.; Jankowski, P.; Liu, Q.; Nitze, F.; Xie, K.; Song, J.; Matic, A. Design of a Multifunctional Interlayer for NASCION-based Solid-State Li Metal Batteries. *Adv. Funct. Mater.* **2020**, *30*, 2001444.

(3) Qiao, Y.; Xu, S.; Liu, Y.; Dai, J.; Xie, H.; Yao, Y.; Mu, X.; Chen, C.; Kline, D. J.; Hitz, E. M.; Liu, B.; Song, J.; He, P.; Zachariah, M. R.; Hu, L. Transient, in situ Synthesis of Ultrafine Ruthenium Nanoparticles for a High-Rate Li-CO_2 Battery. *Energy Environ. Sci.* **2019**, *12*, 1100−1107.

(4) Xie, Z.; Zhang, X.; Zhang, Z.; Zhou, Z. Metal−CO_2 Batteries on the Road: CO_2 from Contamination Gas to Energy Source. *Adv. Mater.* **2017**, *29*, 1605891.
(5) Qiao, Y.; Wu, J.; Zhao, J.; Li, Q.; Zhang, P.; Hao, C.; Liu, X.; Yang, S.; Liu, Y. Synergistic Effect of Bifunctional Catalytic Sites and Defect Engineering for High-Performance Li−CO_2 Batteries. *Energy Storage Mater.* **2020**, *27*, 133−139.
(6) Zhang, Z.; Zhang, Q.; Chen, Y.; Bao, J.; Zhou, X.; Xie, Z.; Wei, J.; Zhou, Z. The First Introduction of Graphene to Rechargeable Li-CO_2 Batteries. *Angew. Chem.* **2015**, *127*, 6650−6653.
(7) Zhang, Z.; Zhao, L.; Xie, Z.; Zhou, Z. Diversified Development of CO_2 in Energy Storage. *Green Chem. Eng.* **2020**, *1*, 79−81.
(8) Pipes, R.; Bhargav, A.; Manthiram, A. Phenyl Disulfide Additive for Solution-Mediated Carbon Dioxide Utilization in Li−CO_2 Batteries. *Adv. Energy Mater.* **2019**, *9*, 1900453.
(9) Du, Y.; Liu, Y.; Yang, S.; Li, C.; Cheng, Z.; Qiu, F.; He, P.; Zhou, H. A Rechargeable All-Solid-State Li−CO_2 Battery using a $Li_{1.5}Al_{0.5}Ge_{1.5}(PO_4)_3$ Ceramic Electrolyte and Nanoscale RuO_2 Catalyst. *J. Mater. Chem. A* **2021**, *9*, 9581−9585.
(10) Li, J.; Zhao, H.; Qi, H.; Sun, X.; Song, X.; Guo, Z.; Tamirat, A. G.; Liu, J.; Wang, L.; Feng, S. Drawing a Pencil-Trace Cathode for a High-Performance Polymer-based Li−CO_2 Battery with Redox Mediator. *Adv. Funct. Mater.* **2019**, *29*, 1806863.
(11) Wang, C.; Zhang, Q.; Zhang, X.; Wang, X.-G.; Xie, Z.; Zhou, Z. Fabricating Ir/C Nanofiber Networks as Free-Standing air Cathodes for Rechargeable Li-CO_2 Batteries. *Small* **2018**, *14*, 1800641.
(12) Hu, A.; Shu, C.; Xu, C.; Liang, R.; Li, J.; Zheng, R.; Li, M.; Long, J. Design Strategies toward Catalytic Materials and Cathode Structures for Emerging Li-CO_2 Batteries. *J. Mater. Chem. A* **2019**, *7*, 21605−21633.
(13) Wang, R.; Zhang, X.; Cai, Y.; Nian, Q.; Tao, Z.; Chen, J. Safety-Reinforced Rechargeable Li-CO_2 Battery Based on a Composite Solid State Electrolyte. *Nano Res.* **2019**, *12*, 2543−2548.
(14) Chen, R.; Li, Q.; Yu, X.; Chen, L.; Li, H. Approaching Practically Accessible Solid-State Batteries: Stability Issues Related to Solid Electrolytes and Interfaces. *Chem. Rev.* **2020**, *120*, 6820−6877.
(15) Thangadurai, V.; Weppner, W. $Li_6ALa_2Nb_2O_{12}$ (A = Ca, Sr, Ba): A New Class of Fast Lithium Ion Conductors with Garnet-like Structure. *J. Am. Ceram. Soc.* **2005**, *88*, 411−418.
(16) Kamaya, N.; Homma, K.; Yamakawa, Y.; Hirayama, M.; Kanno, R.; Yonemura, M.; Kamiyama, T.; Kato, Y.; Hama, S.; Kawamoto, K.; Mitsui, A. A Lithium Superionic Conductor. *Nat. Mater.* **2011**, *10*, 682−686.
(17) Kato, Y.; Hori, S.; Saito, T.; Suzuki, K.; Hirayama, M.; Mitsui, A.; Yonemura, M.; Iba, H.; Kanno, R. High-Power All-Solid-State Batteries Using Sulfide Superionic Conductors. *Nat. Energy* **2016**, *1*, 1−7.
(18) Cheng, L.; Wu, C. H.; Jarry, A.; Chen, W.; Ye, Y.; Zhu, J.; Kostecki, R.; Persson, K.; Guo, J.; Salmeron, M.; Chen, G.; Doeff, M. Interrelationships among Grain Size, Surface Composition, Air Stability, and Interfacial Resistance of Al-Substituted $Li_7La_3Zr_2O_{12}$ Solid Electrolytes. *ACS Appl. Mater. Interfaces* **2015**, *7*, 17649−17655.
(19) Mizuno, F.; Hayashi, A.; Tadanaga, K.; Tatsumisago, M. New, Highly Ion-Conductive Crystals Precipitated from Li_2S-P_2S_5 Glasses. *Adv. Mater.* **2005**, *17*, 918−921.
(20) Liu, Y.; Li, C.; Li, B.; Song, H.; Cheng, Z.; Chen, M.; He, P.; Zhou, H. Germanium Thin Film Protected Lithium Aluminum Germanium Phosphate for Solid-State Li Batteries. *Adv. Energy Mater.* **2018**, *8*, 1702374.
(21) Hu, Y.; Zhong, Y.; Qi, L.; Wang, H. Inorganic/Polymer Hybrid Layer Stabilizing Anode/Electrolyte Interfaces in Solid-State Li Metal Batteries. *Nano Res.* **2020**, *13*, 3230−3234.
(22) Liu, Y.; Li, B.; Kitaura, H.; Zhang, X.; Han, M.; He, P.; Zhou, H. Fabrication and Performance of All-Solid-State Li−Air Battery with SWCNTs/LAGP Cathode. **2015**, *7* (), 17307-17310. DOI: 10.1021/acsami.5b04409.
(23) Li, X.; Zhang, J.; Qi, G.; Cheng, J.; Wang, B. Vertically Aligned N-Doped Carbon Nanotubes Arrays as Efficient Binder-Free Catalysts for Flexible Li-CO_2 Batteries. *Energy Storage Mater.* **2021**, *35*, 148−156.
(24) Zhang, J.; Wang, F.; Qi, G.; Cheng, J.; Chen, L.; Liu, H.; Wang, B. Rechargeable Li-CO_2 Batteries with Graphdiyne as Efficient Metal-Free Cathode Catalysts. *Adv. Funct. Mater.* **2021**, *31*, 2101423.
(25) Zhang, P.-F.; Zhang, J.-Y.; Sheng, T.; Lu, Y.-Q.; Yin, Z.-W.; Li, Y.-Y.; Peng, X.-X.; Zhou, Y.; Li, J.-T.; Wu, Y.-J.; Lin, J.-X.; Xu, B.-B.; Qu, X.-M.; Huang, L.; Sun, S.-G. Synergetic Effect of Ru and NiO in the Electrocatalytic Decomposition of Li_2CO_3 to Enhance the Performance of a Li-CO_2/O_2 Battery. *ACS Catal.* **2020**, *10*, 1640−1651.
(26) Li, X.; Wang, H.; Chen, Z.; Xu, H. S.; Yu, W.; Liu, C.; Wang, X.; Zhang, K.; Xie, K.; Loh, K. P. Covalent-Organic-Framework-Based Li−CO_2 Batteries. *Adv. Mater.* **2019**, *31*, 1905879.
(27) Bie, S.; Du, M.; He, W.; Zhang, H.; Yu, Z.; Liu, J.; Liu, M.; Yan, W.; Zhou, L.; Zou, Z. Carbon Nanotube@RuO_2 as a High Performance Catalyst for Li-CO_2 Batteries. *ACS Appl. Mater. Interfaces* **2019**, *11*, 5146−5151.
(28) Pipes, R.; Bhargav, A.; Manthiram, A. Nanostructured Anatase Titania as a Cathode Catalyst for Li-CO_2 Batteries. *ACS Appl. Mater. Interfaces* **2018**, *10*, 37119−37124.
(29) Zhang, Z.; Yang, C.; Wu, S.; Wang, A.; Zhao, L.; Zhai, D.; Ren, B.; Cao, K.; Zhou, Z. Exploiting Synergistic Effect by Integrating Ruthenium−Copper Nanoparticles Highly Co-Dispersed on Graphene as Efficient Air Cathodes for Li−CO_2 Batteries. *Adv. Energy Mater.* **2019**, *9*, 1802805.
(30) Jin, Y.; Chen, F.; Wang, J.; Johnston, R. L. Tuning Electronic and Composition Effects in Ruthenium-Copper Alloy Nanoparticles Anchored on Carbon Nanofibers for Rechargeable Li-CO_2 Batteries. *Chem. Eng. J.* **2019**, *375*, 121978.
(31) Chen, C. J.; Yang, J. J.; Chen, J. H.; Wei, C. H.; Hu, S. F.; Liu, R. S. Improvement of Lithium Anode Deterioration for Ameliorating Cyclabilities of Non-Aqueous Li-CO_2 Batteries. *Nanoscale* **2020**, *12*, 8385−8396.
(32) Thoka, S.; Tsai, C. M.; Tong, Z.; Jena, A.; Wang, F. M.; Hsu, C. C.; Chang, H.; Hu, S. F.; Liu, R. S. Comparative Study of Li-CO_2 and Na-CO_2 Batteries with Ru@CNT as a Cathode Catalyst. *ACS Appl. Mater. Interfaces* **2021**, *13*, 480−490.
(33) Xiao, Y.; Du, F.; Hu, C.; Ding, Y.; Wang, Z. L.; Roy, A.; Dai, L. High-Performance Li-CO_2 Batteries from Free-Standing, Binder-Free, Bifunctional Three-Dimensional Carbon Catalysts. *ACS Energy Lett.* **2020**, *5*, 916−921.
(34) Inami, Y.; Ogihara, H.; Nagamatsu, S.; Asakura, K.; Yamanaka, I. Synergy of Ru and Ir in the Electrohydrogenation of Toluene to Methylcyclohexane on a Ketjenblack-Supported Ru-Ir Alloy Cathode. *ACS Catal.* **2019**, *9*, 2448−2457.
(35) Tong, Z.; Wang, S. B.; Fang, M. H.; Lin, Y. T.; Tsai, K. T.; Tsai, S. Y.; Yin, L.-C.; Hu, S. F.; Liu, R. S. Na−CO_2 Battery with NASICON-Structured Solid-State Electrolyte. *Nano Energy* **2021**, *85*, 105972.
(36) Key, B.; Schroeder, D. J.; Ingram, B. J.; Vaughey, J. T. Solution-Based Synthesis and Characterization of Lithium-Ion Conducting Phosphate Ceramics for Lithium Metal Batteries. *Chem. Mater.* **2012**, *24*, 287−293.
(37) DeWees, R.; Wang, H. Synthesis and Properties of NaSICON-Type LATP and LAGP Solid Electrolytes. *ChemSusChem* **2019**, *12*, 3713−3725.